ARTICLES

Mesenchymal stem cells within tumour stroma promote breast cancer metastasis

Antoine E. Karnoub[1], Ajeeta B. Dash[2], Annie P. Vo[1], Andrew Sullivan[2], Mary W. Brooks[1], George W. Bell[1], Andrea L. Richardson[3], Kornelia Polyak[4], Ross Tubo[2] & Robert A. Weinberg[1]

Mesenchymal stem cells have been recently described to localize to breast carcinomas, where they integrate into the tumour-associated stroma. However, the involvement of mesenchymal stem cells (or their derivatives) in tumour pathophysiology has not been addressed. Here, we demonstrate that bone-marrow-derived human mesenchymal stem cells, when mixed with otherwise weakly metastatic human breast carcinoma cells, cause the cancer cells to increase their metastatic potency greatly when this cell mixture is introduced into a subcutaneous site and allowed to form a tumour xenograft. The breast cancer cells stimulate *de novo* secretion of the chemokine CCL5 (also called RANTES) from mesenchymal stem cells, which then acts in a paracrine fashion on the cancer cells to enhance their motility, invasion and metastasis. This enhanced metastatic ability is reversible and is dependent on CCL5 signalling through the chemokine receptor CCR5. Collectively, these data demonstrate that the tumour microenvironment facilitates metastatic spread by eliciting reversible changes in the phenotype of cancer cells.

The origins of the invasive and metastatic phenotypes of carcinoma cells have been the subjects of intense investigation. Whereas some current models depict these phenotypes as cell-autonomous alterations specified by the genomes of cancer cells, alternative views propose that metastatic traits are acquired through exposure of epithelial cancer cells to paracrine signals that they receive from mesenchymal cell types within the tumour-associated stroma. Although several lines of evidence demonstrate the contributions of stromal cells to primary tumour growth[1], direct experimental demonstration of the influence of these various cells on the metastatic abilities of cancer cells has been difficult to obtain. This is due, in part, to the complexity of the mesenchymal cell types that are recruited into the stroma, and to the elusive nature of the putative paracrine signals that are exchanged between the mesenchymal and epithelial compartments of a tumour. Recent reports proposed that the bone-marrow-derived mesenchymal stem cell (MSC) is a cell type that is recruited in large numbers to the stroma of developing tumours[2]. To characterize better the role of this stromal cell in tumorigenesis, we set out to determine whether MSCs could supply contextual signals that serve to promote cancer metastasis.

Mesenchymal stem cells are pluripotent progenitor cells that contribute to the maintenance and regeneration of a variety of connective tissues, including bone, adipose, cartilage and muscle[3]. Although MSCs reside predominantly in the bone marrow, they are also distributed throughout many other tissues, where they are thought to serve as local sources of dormant stem cells[4,5]. The contributions of MSCs to tissue formation become apparent only in cases of tissue remodelling after injury or chronic inflammation. These conditions are typically accompanied by the release of specific endocrinal signals from the injured or inflamed tissue that are then transmitted to the bone marrow, leading to the mobilization of multi-potent MSCs and their subsequent recruitment to the damage site[6]. For example, MSCs have been shown to contribute to the formation of fibrous scars after injury[7].

The formation of breast carcinomas is often accompanied by a well-orchestrated desmoplastic reaction, which involves the recruitment of a variety of stromal cells with both pro- and anti-tumorigenic activities[1]. Such response closely resembles wound healing and scar formation, and entails the constant deposition of growth factors, cytokines and matrix-remodelling proteins that render the tumour site a 'wound that never heals'[8]. This suggests that, similar to sites of injury, actively growing tumours recruit MSCs through the release of various endocrine and paracrine signals. Indeed, as we have found, mouse stroma prepared from developing human MCF7/Ras or MDA-MB-231 breast cancer xenografts is rich in cells with an ability to generate fibroblastoid colony-forming units (CFU-F) *in vitro* (Supplementary Fig. 1a), a hallmark of MSCs[3]. The absence of such colonies from control Matrigel plugs or from neighbouring tissues (negative control; Supplementary Fig. 1a) suggested that endogenous murine MSCs localize specifically to sites of neoplasia.

To investigate whether human breast cancer cells also have the ability to attract human MSCs, we established a transwell assay in which bone-marrow-derived human MSCs were allowed to migrate towards media derived from MCF7/Ras or MDA-MB-231 cultures. We found that human MSCs migrated much more avidly (~11-fold more) towards media derived from these cancer cells than towards control media (Supplementary Fig. 1b). More importantly, green fluorescent protein (GFP)-labelled human MSCs infused into the venous circulation of mice bearing MCF7/Ras or MDA-MB-231 human breast cancer xenografts localized specifically to the developing tumours, with no observable accumulation in other tissues, such as the kidneys (Supplementary Fig. 1c), liver and spleen (data not shown). Such findings indicated that MSCs are specifically recruited by subcutaneous breast xenografts, and corroborated recent studies that described the localization of systemically infused MSCs to other types of malignancy, such as gliomas[9,10], colon carcinomas[11,12], ovarian carcinomas[13], Kaposi's sarcomas[14] and melanomas[15].

[1]Whitehead Institute for Biomedical Research and Massachusetts Institute of Technology, Cambridge, Massachusetts 02142, USA. [2]Genzyme Corporation, Framingham, Massachusetts 01701, USA. [3]Department of Pathology, Brigham and Women's Hospital, Boston, Massachusetts 02115, USA. [4]Department of Medical Oncology, Dana-Farber Cancer Institute, Harvard Medical School, Boston, Massachusetts 02115, USA.

MSCs enhance breast cancer metastasis

To investigate the functional consequences of the heterotypic interactions between MSCs and mammary carcinoma cells, we established a xenograft model in which GFP-labelled MCF7/Ras, MDA-MB-231, MDA-MB-435 and HMLER (see Methods) human breast cancer cells (BCCs) were mixed with bone-marrow-derived human MSCs (hereafter referred to as MSCs) and injected subcutaneously into immunocompromised mice. The growth kinetics of the MSC-containing tumours (BCCs plus MSCs) were compared to those of BCCs injected alone (BCCs) over the subsequent 8–12 weeks, after which the histopathology of the resulting tumours was studied.

We found that MSCs accelerated the growth of MCF7/Ras tumours without affecting the kinetics of MDA-MB-231-, MDA-MB-435- or HMLER-containing tumours (Fig. 1a). More importantly, whereas mice carrying tumours composed only of BCCs exhibited few microscopic metastases in the lungs (Fig. 1b, d), mice bearing the mixed MCF7/Ras+MSC, MDA-MB-231+MSC, MDA-MB-435+MSC and HMLER+MSC tumours displayed a marked increase in the numbers of micro- and macroscopic lung metastases (Fig. 1b, d). Normalized counts of the metastatic nodules in the lungs of BCC+MSC-bearing mice compared to their BCC-control littermates revealed two-, three-, four- and sevenfold enhancements in the overall numbers of detectable HMLER, MDA-MB-435, MCF7/Ras and MDA-MB-231 metastatic deposits, respectively (Fig. 1c). Furthermore, in contrast to the MDA-MB-231-bearing mice, the MDA-MB-231+MSC-bearing mice showed metastases to various other tissues, including the mammary glands (Supplementary Table 1). Although all four of the tested cell lines exhibited enhanced metastatic potential after admixture of MSCs, we chose to focus further analysis on the MDA-MB-231 tumour model, because it displayed the greatest relative increase in MSC-induced metastasis without any concomitant effect on either tumour cell proliferation (as revealed by Ki67 staining; Supplementary Fig. 2) or overall primary tumour growth kinetics.

We note that admixture of other types of mesenchymal cells—specifically WI-38 or BJ human fibroblasts (Supplementary Fig. 3 and data not shown)—to MDA-MB-231 cancer cells before injection into host mice did not result in either enhanced growth kinetics (Supplementary Fig. 3a, b) or increased numbers of lung metastases (Supplementary Fig. 3c, d). Taken together, these observations indicated that the metastasis-enhancing powers were a specific property of admixed MSCs or derivatives thereof.

Reversible metastasis

Implantation of MSCs either contralaterally to MDA-MB-231 cells or in nearby separate sites of injection did not affect the metastatic potential of the resulting primary tumours (data not shown), indicating that MSCs could enhance cancer metastasis only when they were in close proximity to the engrafted BCCs. This influence might be ascribed to various effects that MSCs exert on the commingled carcinoma cells. Thus, the MSCs might favour the outgrowth of rare variants within the MDA-MB-231 cell populations that exhibit unusually high metastatic powers. Alternatively, the MSCs might cause otherwise weakly metastatic MDA-MB-231 cells to acquire enhanced metastatic abilities. This latter mechanism suggests the possibility that the acquisition of the metastatic phenotype might be reversible, in that carcinoma cells might revert to a lower metastatic state once they were no longer in close contact with MSCs.

To resolve between these two mechanisms, explants of MDA-MB-231 cells were prepared from BCC plus MSC primary tumours (T-explants) as well as from their derived lung metastases (L-explants), expanded *in vitro*, cleared from contaminating stromal components, and then re-injected into subcutaneous sites in host mice in order to evaluate their respective metastatic powers (Fig. 2a). Although the growth rate of the resulting L-explant primary tumours was marginally enhanced compared to their T-explant counterparts (Fig. 2b, c), these L-explant cells were no more metastatic than the parental T-explant cancer cells (Fig. 2d). This suggested that the

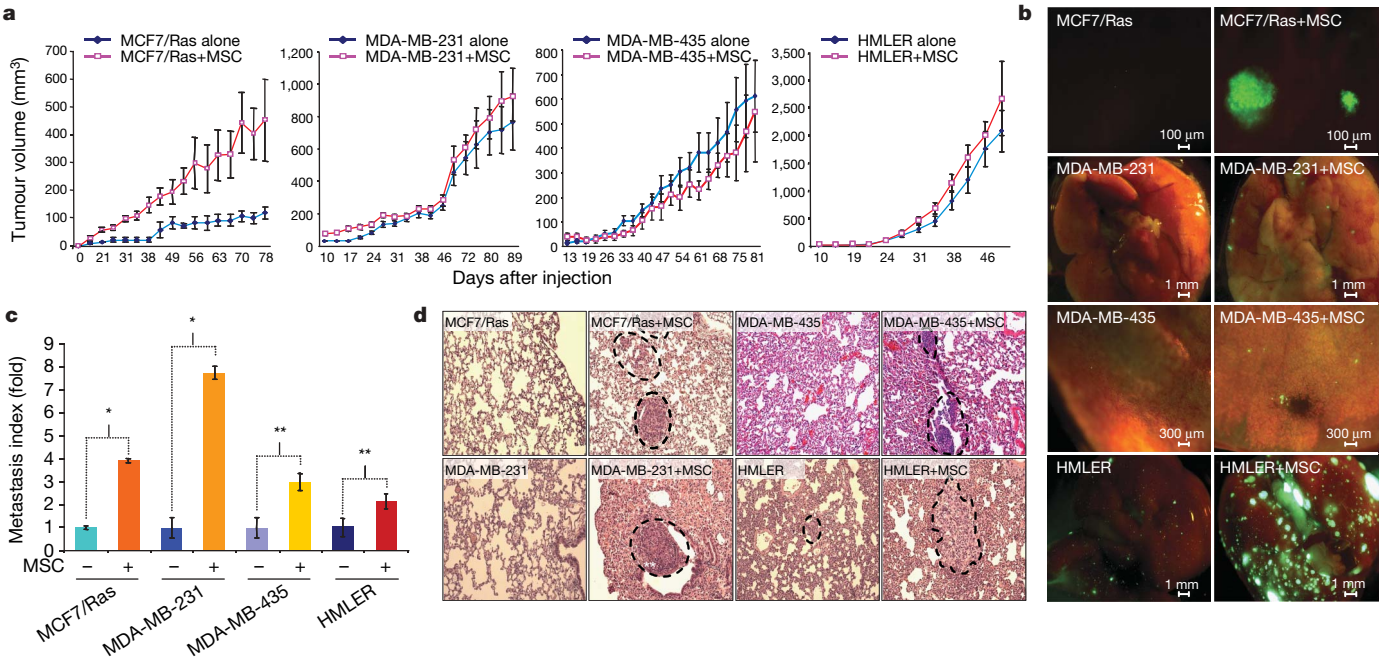

Figure 1 | MSCs promote breast cancer metastasis. **a**, Tumour volume measurements (mean ± s.e.m.) of 500,000 GFP-labelled BCCs injected subcutaneously into nude mice with or without 1.5×10^6 MSCs. Representative data from multiple experiments are shown. Diamonds, BCCs alone, $n = 5$–7 mice per group; squares, BCCs plus MSCs, $n = 5$–8 mice per group. **b**, Representative bright-field/fluorescence images of lungs of mice bearing the indicated tumours. Cancer colonies are in green. MCF7/Ras-bearing mice were killed at approximately day 150 to allow these tumours to grow to comparable sizes to their MCF7/Ras+MSC counterparts. **c**, The lung metastasis indices pooled within each cohort of mice in **a** are expressed as fold increase (±s.e.m.) over controls. Data shown are representative of multiple repeats. Asterisk, $P < 0.01$, double asterisk, $P < 0.05$ using one-tailed Student's *t*-test. **d**, Representative haematoxylin-and-eosin-stained sections of lungs of mice bearing the indicated tumours. Metastases are delineated by a dashed line.

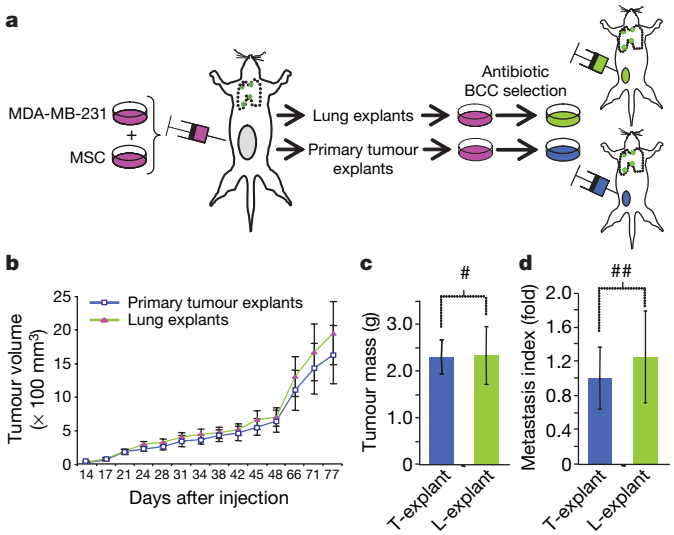

Figure 2 | MSC-induced increase in the metastasis of MDA-MB-231 cells involves reversible mechanisms. **a**, BCCs were recovered from lung or primary tumour tissues, cleared of stromal contaminants by culture in blasticidin-containing media (5 μg ml^{-1}), and re-injected as primary subcutaneous tumours in recipient animals. **b**, Tumour growth (means ± s.e.m.) of 500,000 GFP-labelled lung-derived (L-explant) or primary tumour-derived (T-explant) MDA-MB-231 cells inoculated subcutaneously. Data shown are representative of multiple independent experiments in which four different paired batches of L-explant and T-explant cultures were assayed in parallel. MDA-MB-231-T-explant ($n = 8$ mice); MDA-MB-231-L-explant ($n = 10$ mice). **c**, Masses (means ± s.e.m.) of tumours in **b**. Hash, $P > 0.4$ using one-tailed Student's *t*-test and indicates no statistical significance. **d**, Lung metastasis index of mice in **c**. Double hash, $P > 0.3$ using one-tailed Student's *t*-test and indicates no statistical significance.

MSC-induced metastatic powers reflected a reversibly induced trait of the MDA-MB-231 cells, and that the ability of these cells to metastasize to the lungs was a consequence of their 'education' by MSCs in the primary tumour rather than the selection of rare variants of MDA-MB-231 cells that display elevated metastatic potency in a stable fashion.

The effects that the MSCs exerted on the BCCs might have occurred within the site of primary tumour formation. Alternatively, the MSCs might have accompanied the metastasizing BCCs to sites of metastasis formation. To distinguish between these two possibilities, we admixed ds-red-labelled MSCs to GFP-labelled MDA-MB-231 cells and implanted the mixture subcutaneously in host mice. We found that the tumour-derived lung metastases contained green-labelled MDA-MB-231 cells but no detectable red-labelled MSCs (or their derivatives; Supplementary Fig. 4a) when scored 4, 5 or 6 weeks after primary tumour implantation. The absence of red-labelled MSCs from the lung metastatic sites cannot be ascribed to an inhospitable lung parenchyma, as MSCs that lodge in the lungs of recipient animals after tail-vein infusion survive in that environment for ~6 weeks after injection (Supplementary Fig. 4b). Hence, it appeared that the admixed MSCs do not migrate in large numbers to the sites of metastasis, and that they exerted their pro-metastatic effects on BCCs in the context of primary tumours.

CCL5 in MSC-induced metastasis

The aforementioned observations indicate that MSCs supply locally acting paracrine cues that induce BCCs within primary tumours to metastasize. To understand this crosstalk better, *in vitro* co-cultures of MDA-MB-231 breast cancer cells and MSCs were established and their conditioned media were screened for the levels of various cytokines, chemokines and growth factors using the Luminex-based Bio-Plex suspension array system (Fig. 3a). In some cases, the resulting

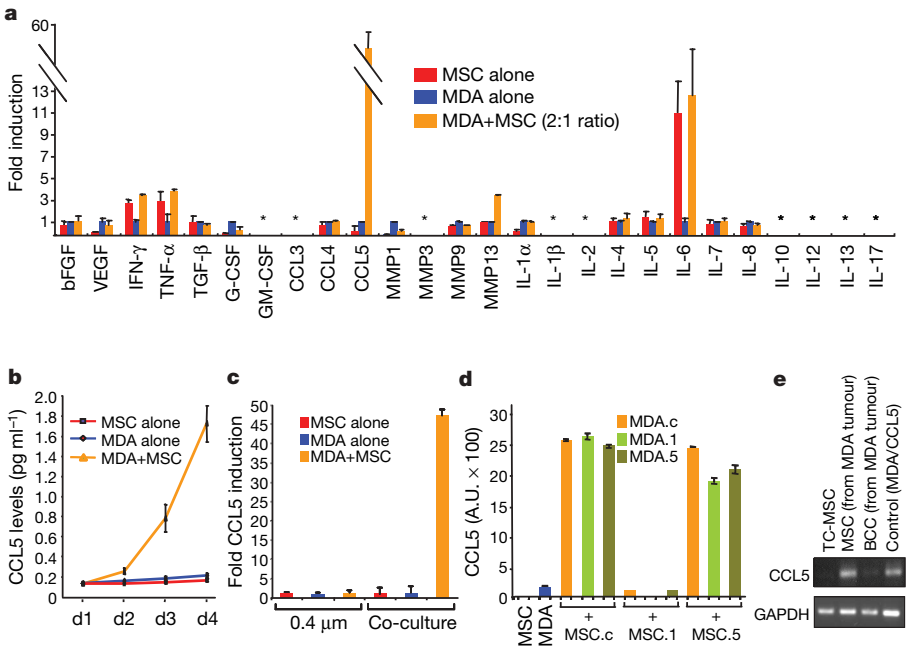

Figure 3 | The interaction of BCCs with MSCs causes a rise in the levels of CCL5. **a**, MDA-MB-231, MSCs, or MDA-MB-231+MSCs were cultured in complete media for 3 days. The levels of various factors in the cell-free culture supernatants were measured by xMAP Bio-Plex cytokine arrays at day 3, and were normalized to the levels observed in the media of BCCs cultured alone. Data are expressed as fold induction ± s.d. of triplicates. Asterisk indicates undetectable levels. **b**, CCL5 ELISA on the media of MDA-MB-231, MSCs, or MDA-MB-231+MSC cultures (1:3 MDA:MSCs) at the indicated time points. Data points represent means ± s.d. of quadruplicates. **c**, BCCs were separated from co-cultured MSCs by a 0.4-μm membrane. CCL5 levels were probed by ELISA on the culture supernatants. Data are expressed as fold induction over levels seen in MDA-MB-231 culture supernatants (mean ± s.d. of triplicates). **d**, CCL5 ELISA on the supernatants of MSC-siluc (MSC.c), MSC-siCCL5.1 (MSC.1) and MSC-siCCL5.5 (MSC.5) co-cultured with MDA-MB-231-siluc (MDA.c), MDA-MB-231-siCCL5.1 (MDA.1), or MDA-MB-231-siCCL5.5 (MDA.5). Data are expressed as means ± s.d. of triplicates in arbitrary units (A.U.). **e**, RT–PCR analyses of CCL5 in MSCs and BCCs sorted from GFP–MSC+MDA-MB-231 tumours (3:1 ratio) 4 weeks after tumour implantation. Tissue-cultured MSCs (TC-MSC) and MDA-MB-231/CCL5 cells were used as controls. GAPDH was used for equal loading.

levels of certain released factors (for example, interferon-γ or tumour-necrosis factor-α) reflected the additive contributions of the two cell types when cultured on their own. Notably, the levels of only one cytokine, CCL5, reflected a synergistic interaction between the MSCs and BCCs, as it accumulated to levels ~60-fold higher than those produced by pure BCC cultures (Fig. 3a). This cooperative induction of CCL5 was proportional to the numbers of MSCs mixed with the BCCs (Supplementary Fig. 5a), and was apparent as early as the third day of co-culture (Fig. 3b). Moreover, this induction required close physical contact between MSCs and cancer cells, because it failed to occur when the two cell populations were separated by a permeable membrane (Fig. 3c).

We undertook to determine the source of the CCL5 produced under conditions of co-culture. To do so, we stably reduced the expression of CCL5 in MDA-MB-231 cells by >80% using short hairpin (sh)RNA (variant siCCL5.1; Supplementary Fig. 6). Importantly, however, subsequent co-culture of these MDA-MB-231.1 cells with MSCs continued to allow accumulation of CCL5 in the culture supernatants to levels that were comparable to those observed in the co-cultures of MSCs and control cancer cells (Fig. 3d). This suggested that the source of CCL5 was the admixed neighbouring MSCs. Indeed, inhibition of CCL5 protein expression in MSCs using the same shRNA hairpin vector (MSC.1; Fig. 3d) resulted in more than 75% reduction of CCL5 protein levels in the co-cultures, indicating that the MSCs were the major source of the CCL5 observed on co-culture of the two cell types. In support of this conclusion, analysis of CCL5 levels in the media of MSCs or MDA-MB-231 cells separated from one another after 3 days of co-culture indicated a strong induction of CCL5 in the culture of MSCs, but not that of BCCs (Supplementary Fig. 5b). Finally, polymerase chain reaction with reverse transcription (RT–PCR) analysis of the RNA prepared from these co-culture-derived MSCs (Supplementary Fig. 5c), as well as from the MSCs isolated from MDA-MB-231+MSC tumours ~4 weeks after tumour implantation (Fig. 3e), indicated a strong accumulation of *CCL5* messenger RNA, suggesting that an active signal transduction pathway is triggered in MSCs by the nearby BCCs.

A series of observations has linked CCL5 signalling and cancer. For example, CCL5 levels in the plasma of breast cancer patients have been correlated with the severity of the disease, and localized CCL5 protein expression was found to be elevated in invasive tumours when compared to *in situ* ductal tumours or benign lesions[16,17]. However, the precise contributions of CCL5 to cancer development and progression are poorly understood. To investigate further the possible causal role of CCL5 in cancer cell metastasis, we overexpressed this chemokine in the MDA-MB-231 BCCs (Supplementary Fig. 7a) and analysed its effects on cancer cell growth and tumorigenesis. The overexpressed CCL5 did not confer any proliferative advantage on cultured cancer cells when compared with those lacking such overexpression (Supplementary Fig. 7b), and had no effect on the ability of BCCs either to grow in an anchorage-independent fashion *in vitro* (Supplementary Fig. 7c), or to form primary subcutaneous tumours in immunocompromised mice (Fig. 4a). However, these tumours exhibited a ~5-fold enhancement in their metastatic potential when compared with control tumours lacking ectopic CCL5 (Fig. 4a). Similarly, overexpression of CCL5 in WI-38 fibroblasts sufficed to enable these cells to promote the metastasis of admixed MDA-MB-231 BCCs (Fig. 4b), indicating that the actions of CCL5 are responsible for much, if not all, of the observed MSC-induced metastasis by the BCCs.

CCL5 promotes lung colonization

Previous reports have described an important role for CCL5 as a chemoattractant for stromal cells, such as macrophages, that express one of the receptors for CCL5, CCR5 (refs 18, 19). Furthermore, CCL5 expression has been associated with increased tumour neovascularization, suggesting that endothelial cells, which express a variety of chemokine receptors, may also be attracted by CCL5 to sites of tumour formation, thereby enhancing tumour angiogenesis[20]. Such observations suggest that CCL5 may contribute to breast cancer metastasis through the recruitment of a number of stromal cell types to sites of primary tumour growth.

However, immunohistochemical analyses indicated that the MDA-MB-231 control and CCL5-overexpressing MDA-MB-231 (MDA-MB-231/CCL5) tumours exhibited comparable numbers of tumour-infiltrating macrophages and had similar vessel densities (as evident by F4/80 and MECA-32 staining for macrophages and endothelial cells, respectively; Supplementary Fig. 8). In addition, we found that ectopic CCL5 expression did not cause an accumulation of other stromal cells, such as SMA-positive cells, in the examined tumours (Supplementary Fig. 8a). Together, these data indicated that the observed CCL5-induced metastasis could not be attributed to significant effects on the numbers of the major constituents of the stroma or to the vascularity of these tumour xenografts.

Invasion and metastatic dissemination of carcinoma cells are often facilitated by their transdifferentiation through the process termed

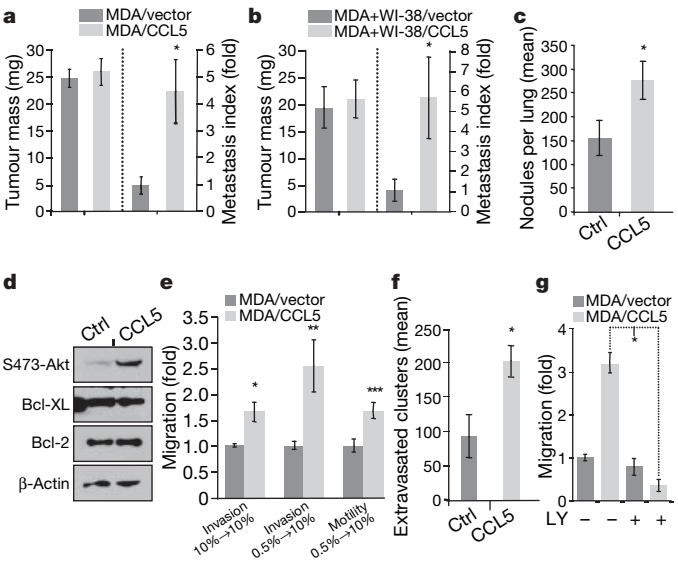

Figure 4 | CCL5 enhances breast cancer cell migration, invasion and metastasis. **a**, A total of 500,000 MDA-MB-231/vector (ctrl) or MDA-MB-231/CCL5 cells were injected subcutaneously in NOD/SCID mice. Tumour masses (mean ± s.e.m., $n = 6$ each group) were taken at 10 weeks. Lung metastasis indices are expressed as fold increase (±s.e.m.) over controls. Data shown are representative of multiple repeats. Asterisk, $P < 0.01$ in one-tailed Student's *t*-test. **b**, A total of 500,000 MDA-MB-231 cells were admixed to 250,000 WI-38 fibroblast controls (WI-38/vector) or WI-38 fibroblasts overexpressing CCL5 (WI-38/CCL5) and were injected subcutaneously in NOD/SCID mice. Tumours ($n = 5$ per group) were excised and weighed at 12 weeks. Masses shown represent mean ± s.e.m. Lung metastasis indices are expressed as fold increase (±s.e.m.) over controls. Asterisk, $P < 0.01$ in one-tailed Student's *t*-test. **c**, A total of 800,000 indicated BCCs were introduced into the circulation of NOD/SCID hosts. GFP-positive cancer colonies in the lungs were counted 6.5 weeks later. Bars represent means ± s.e.m. (MDA-MB-231 controls, $n = 16$ mice; MDA-MB-231/CCL5, $n = 18$ mice). Asterisk, $P < 0.01$ in one-tailed Student's *t*-test. **d**, Western blot analysis of lysates of MDA-MB-231 control or MDA-MB-231/CCL5 cells. β-Actin was used as a loading control. **e**, Transwell migration or Matrigel invasion assays on 50,000 MDA-MB-231 control or MDA-MB-231/CCL5 cells. Data are representative of multiple independent experiments and are expressed as means ± s.d. Asterisk, $P < 0.05$; double asterisk, $P < 0.05$; triple asterisk, $P < 0.01$ in one-tailed Student's *t*-test. **f**, One million GFP-labelled BCCs were injected into the tail vein of NOD/SCID mice. Lungs were processed 48 h later and examined for extravasated cells. Bars represent means ± s.e.m. (MDA-MB-231 cells, $n = 7$ mice; MDA-MB-231/CCL5, $n = 10$ mice). Asterisk, $P < 0.01$ in one-tailed Student's *t*-test. **g**, Transwell migration assays on 50,000 MDA-MB-231 control or MDA-MB-231/CCL5 cells plated with or without the phosphatidylinositol-3-OH kinase inhibitor LY290042 (0.5 μM); representative experiment shown; asterisk, $P < 0.01$ in one-tailed Student's *t*-test.

the epithelial-to-mesenchymal transition (EMT), in which cells shed their epithelial characteristics and acquire instead a series of mesenchymal markers that enable their invasiveness and intravasation[21]. Despite their lack of E-cadherin and their expression of detectable levels of mesenchymal markers such as fibronectin (data not shown), the MDA-MB-231 cells studied here exist in an intermediary phenotypic state of 'partial EMT', as they retain a distinctive epithelial morphology *in vitro* and are still responsive to EMT-inducing stimuli in culture. In fact, we observed that ectopic CCL5 expression did not cause MDA-MB-231 cells to undergo the morphological changes usually associated with an EMT (Supplementary Fig. 9a), did not cause rearrangement of their actin cytoskeleton (Supplementary Fig. 9b), and had no impact on the expression of mesenchymal markers closely associated with the EMT process, namely vimentin, N-cadherin (Supplementary Fig. 9c) and fibronectin (data not shown). These data suggested that CCL5 does not directly promote the EMT programme of MDA-MB-231 cells.

We proceeded to explore an alternative possibility: that CCL5 expression affected some of the later, critical steps of the invasion–metastasis cascade, namely the lodging of cancer cells in secondary organs and the subsequent step of colonization. For that purpose, MDA-MB-231/CCL5 cells were injected intravenously into host mice, and the lungs of these hosts were examined ~6 weeks later using fluorescence microscopy. These experiments revealed that CCL5-overexpressing cells indeed had a significant ~1.8-fold advantage over their control counterparts in colonizing the lungs (Fig. 4c), suggesting that CCL5 exposure has effects on later steps of the invasion–metastasis cascade. We note once again that this enhanced tissue-colonizing ability was not due to CCL5's effects on cellular proliferation measured either *in vitro* (Supplementary Fig. 7b) or *in vivo* (Supplementary Fig. 7g, Ki67 staining).

Because improved colonization can be due to enhanced cellular survival, we tested whether CCL5 protects against apoptosis. Notably, we found that MDA-MB-231/CCL5 cells exhibited higher levels of the Ser 473-phosphorylated, activated form of Akt, but exhibited no difference in the levels of other pro-survival proteins, such as Bcl-XL or Bcl-2 (Fig. 4d), or a reduction in the levels of pro-apoptotic molecules such as BAX or BAD (data not shown). Moreover, we found that overexpression of CCL5 had no effect on the ability of MDA-MB-231 cells to withstand serum deprivation (Supplementary Fig. 7b), loss of substrate anchorage (Supplementary Fig. 7d), or hyperoxia (data not shown). We also observed that ectopic CCL5 expression did not protect MDA-MB-231 cells from doxorubicin-induced apoptosis monitored using western blots for cleaved caspase-3 (CC3) and cleaved PARP (as markers of apoptosis; Supplementary Fig. 7e), or TdT-mediated dUTP nick end labelling (TUNEL) assays (Supplementary Fig. 7f). Finally, immunohistochemical analyses on control and CCL5-overexpressing tumours revealed only minor differences in the levels of apoptotic CC3-positive cancer cells among the examined groups (Supplementary Fig. 7g, h). Together, these observations suggested that CCL5 does not exert any detectable pro-survival functions *in vitro* or *in vivo*, and that the observed enhancement of lung colonization was not a consequence of significant anti-apoptotic activities of CCL5.

Akt serves as a key relay switch for upstream signals that promote both cell survival as well as cellular motility[22]. Because CCL5-induced Akt phosphorylation did not correlate with enhanced protection against apoptosis, we tested whether the CCL5-enhanced lung colonization could be due to an increased ability of MDA-MB-231/CCL5 cells to invade from the microvasculature into the lung parenchyma through the process of extravasation. Indeed, ectopic expression of CCL5 enhanced the motility of MDA-MB-231 cells through permeable Boyden chamber membranes by ~1.5-fold as well as the invasion of these cells through Matrigel layers by ~1.6 or ~2.5-fold in either high or low serum conditions, respectively (Fig. 4e). Notably, when we flushed the lungs of mice 48 h after BCC tail-vein injection—in order to remove most cells that remained within the microvasculature of the lungs and thus had not extravasated—we found twice as many deposits in the MDA-MB-231/CCL5-injected group than their control-injected littermates (Fig. 4f). This indicates a clear effect of CCL5 on cancer cell extravasation.

Finally, we investigated the role of Akt in mediating the actions of CCL5 on cellular motility by using the phosphatidylinositol-3-OH

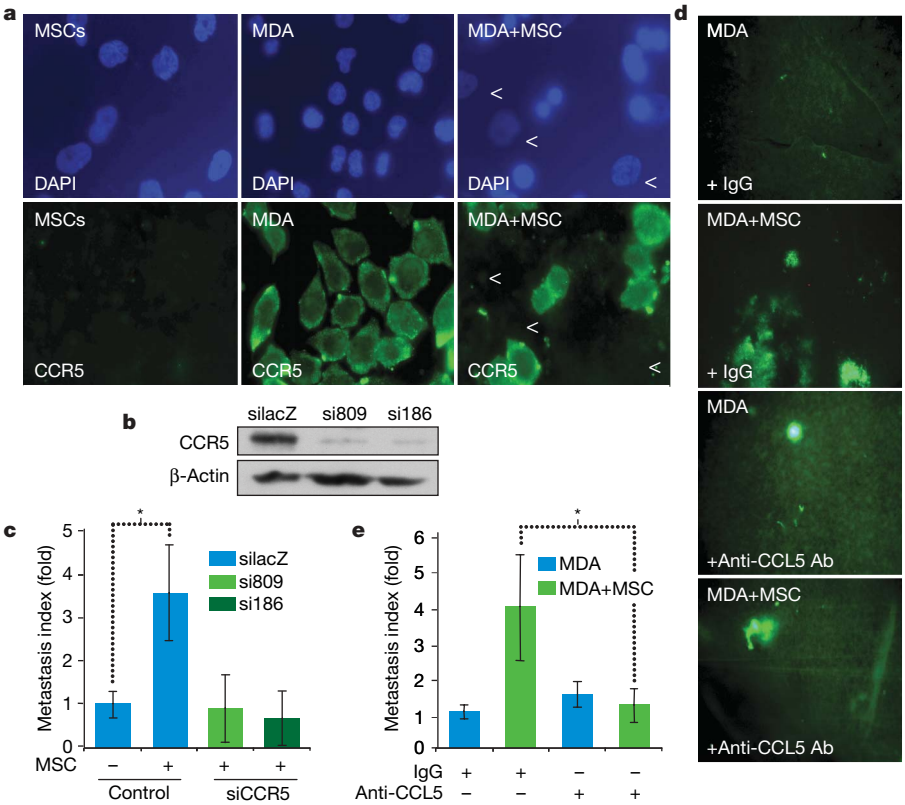

Figure 5 | CCL5–CCR5 interaction is essential for the MSC-induced metastasis. **a**, Immunofluorescence analysis of CCR5 distribution in MDA-MB-231 cells cultured with MSCs. DAPI (for nuclei staining) is in blue; CCR5 detected in green. Arrowheads denote MSCs. **b**, Western blot analysis showing CCR5 expression in MDA-MB-231/silacZ, MDA-MB-231/siCCR5(809) and MDA-MB-231/siCCR5(186) lysates. β-Actin was used as a loading control. **c**, A total of 500,000 cells of the MDA-MB-231 variants in **b** were co-mixed with 1.5×10^6 MSCs and injected subcutaneously into nude mice. Mice were killed when tumours reached 1 cm in diameter and the metastasis index was calculated for each cohort ($n = 5$ per group). Results represent means ± s.e.m.; asterisk, $P < 0.05$ using one-tailed Student's *t*-test. **d**, Anti-CCL5 neutralizing antibody or control IgG was administered intraperitoneally twice weekly in SCID mice bearing MDA-MB-231 ($n = 9$) or MDA-MB-231+MSC tumours ($n = 11$). Representative lung pictures of the indicated cohorts are shown. **e**, Lung metastasis indices of mice in **d**. Data shown are representative of means ± s.e.m. Asterisk, $P < 0.05$ in one-tailed Student's *t*-test.

kinase inhibitor LY294002. Drug concentrations that did not inhibit the basal motility levels of MDA-MB-231 cells blocked the elevation of motility induced by ectopic CCL5 expression (Fig. 4g). These results, when taken together, suggest that the observed CCL5-enhanced lung colonization could be ascribed, in significant part, to its ability to promote extravasation and/or motility of cancer cells at sites of dissemination rather than promoting the survival and/or proliferation of these cells.

Essential role for the CCL5–CCR5 loop

CCL5 acts through three G-protein-coupled receptors, termed CCR1, CCR3 and CCR5 (ref. 23). CCR5 has been determined to be the main receptor for CCL5 in MDA-MB-231 cells, as inhibition of its surface expression through dominant-negative mutants abrogated the ability of these cells to respond to CCL5 chemotaxis[24]. We therefore focused our efforts on evaluating the importance of the CCL5–CCR5 interactions in MSC-induced metastasis.

We confirmed that CCR5 is expressed by MDA-MB-231 cells and not by MSCs (Fig. 5a), supporting the notion that MSC-derived CCL5 acts primarily in a paracrine fashion on MDA-MB-231 cells in the BCC and MSC mixed cell populations described above. To probe whether the observed MSC-induced metastasis required CCL5–CCR5 interactions, we inhibited CCR5 expression in MDA-MB-231 cells by more than 85% through shRNA knockdown (ref. 25 and Fig. 5b), and mixed these cells with MSCs before implantation into host mice. Indeed, inhibition of CCR5 expression in the BCCs, achieved using either of two different shRNA constructs, abrogated the ability of MSCs to enhance the metastasis of MDA-MB-231 cells (Fig. 5c). Furthermore, neutralization of CCL5 protein using intraperitoneal injections of an anti-human CCL5 monoclonal antibody also abrogated the MSC-induced metastasis by MDA-MB-231 cells (Fig. 5d, e). In addition, MSCs in which CCL5 expression was inhibited by shRNA knockdown failed to promote metastasis of the admixed MDA-MB-231 cells (data not shown). Taken together, these results underscore the critical importance of the CCL5–CCR5 paracrine interactions in enabling MSCs to induce metastasis of the MDA-MB-231 cells.

Discussion

Certain models of metastatic progression propose that cancer cell invasion and metastasis from the primary tumour site are strongly influenced by contextual signals emanating from the stroma of the primary tumour. It follows that if carcinoma cells are subsequently deprived of such signals, they may revert to an earlier phenotypic state in which they no longer display the traits of high-grade malignancy. Indeed, such a model has been proposed previously by others on the basis of indirect evidence[21]. Here, we demonstrate that at least one mesenchymal cell type, the MSC, can expedite tumour metastasis, and suggest that after primary human carcinomas recruit MSC populations into their midst, subsequent interactions between the MSCs (or their derivatives) and the BCCs endow the latter with invasive and metastatic properties.

Although the recruitment of labelled MSCs to tumour xenografts has been established in a variety of experimental models of tumorigenesis, there is currently no available way to quantify with any accuracy the number of MSCs in actual human tumours, in part because no set of markers has been identified that can uniquely stain these cells without concomitantly staining other mesenchymal types in the tumour-associated stroma[6]. Our demonstration that the stroma derived from tumour xenografts contained appreciable numbers of murine MSCs indicates that significant steady-state levels of these cells are maintained in developing tumours. Interestingly, the use of CD10—one of the markers associated with human MSCs—to purify cells from the stroma of human primary invasive breast carcinomas yielded a population of cells that expresses a number of other markers collectively used to characterize human MSCs (for example, CD44, CD105 and CD106; Fig. 6a). This suggested that, similar to tumour xenografts, human carcinomas also acquire significant numbers of MSCs. Furthermore, we note that CCL5, which is prominent in the stromal gene expression signature associated with poor prognosis of breast cancers[26] (SFT; Fig. 6b, c), is also enriched in the leukocyte- and endothelial cell-free stroma of primary invasive ductal carcinomas (Fig. 6d), specifically in the CD10-positive compartment[27] (Fig. 6e). Collectively, these observations argue strongly for a significant association between stromal CCL5 levels, MSCs and human invasive breast cancers.

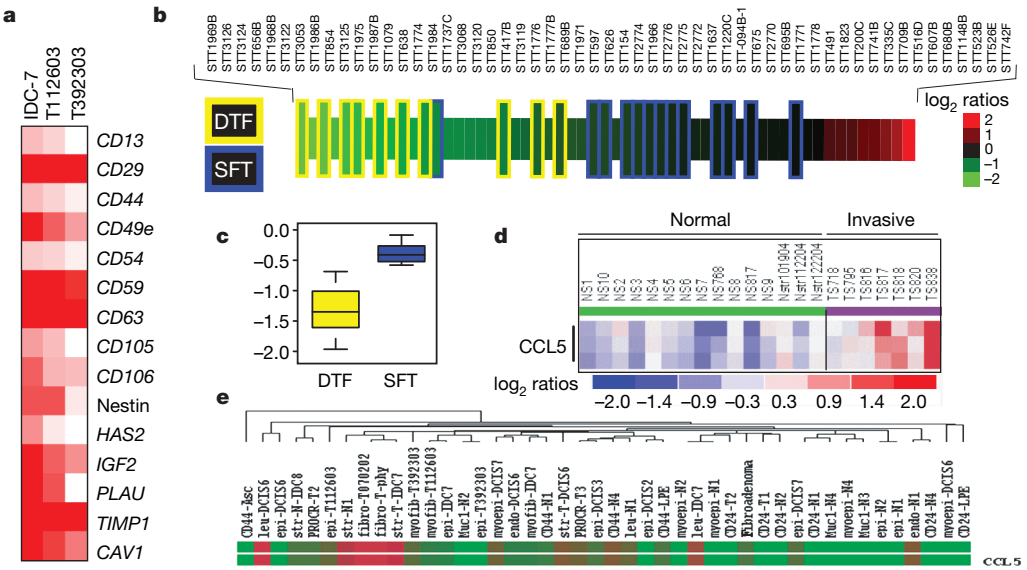

Figure 6 | Stromal fibroblastic cells of human invasive ductal carcinomas are rich in MSC markers and overexpress CCL5. **a**, SAGE TreeView display of MSC markers expressed in stromal CD10-positive cells from invasive tumours[27]. **b**, Soft-tissue tumours were ranked by CCL5 expression[26], from low (green) to high (red). Wide blocks indicate expression ratios of tumours classified as desmoid-type fibromatosis (DTF; yellow outline, $n = 10$) or solitary fibrous tumours (SFT; blue outline, $n = 13$); narrow blocks are other soft-tissue tumours ($n = 32$). **c**, Box plot showing that CCL5 expression is higher ($P = 0.004$) in SFT than in DTF. The difference in $\log_2$ expression ratios between SFT and DTF was tested with the Welch's test. **d**, CCL5 Affymetrix gene expression in the stroma of human invasive ductal cancers compared to that in normal cancer-free breast tissue (indicated as 'Normal'; see Methods). **e**, CCL5 expression is mostly restricted to the CD10-positive fibroblastic cells derived from invasive ductal cancers. The heatmap shown is a cluster of CCL5.genelist obtained as in **a**. Details of the purification methodologies of the various groups indicated in **a**, **d** and **e** are found in ref. 27.

Although we have focused here on CCL5 in the MSC–MDA-MB-231 cell interactions, CCL5 seems to have an equally critical involvement in the functional interaction of MSCs with MDA-MB-435 human BCCs. CCL5 levels accumulate synergistically when the two cell types are co-cultured together (Supplementary Fig. 10a), and MSCs in which CCL5 expression was compromised by shRNA knockdown failed to promote metastasis by MDA-MB-435 cells to which they were admixed (Supplementary Fig. 10b). With these facts in mind, we point out that CCL5 does not seem to be involved in regulating the MSC-induced metastasis of MCF7/Ras or HMLER cells, which may depend on other paracrine factors such as VEGF and interleukin-8. Nevertheless, our observations highlight the recently discovered critical roles of chemokine networks in malignant progression[28,29] and suggest the possible utility of a variety of CCL5 analogues and CCR5 antagonists currently used in anti-HIV therapy[30] in treating metastatic disease.

Notably, we have observed that MSCs induce the metastasis of cells to the lung that are, on isolation and re-injection into recipient mice, no more metastatic than their predecessors in the primary tumour (Fig. 2e). This indicated that acquisition of increased metastatic powers by these tumour cells was reversible, and suggested that the maintenance of this phenotype depends on continuing contact with stromal cells. If extended to other tumour types, the present results hold important implications for the molecular analysis of malignant progression. They suggest that many of the cellular functions associated with invasion and metastasis are often not expressed constitutively by carcinoma cells, but rather only transiently in response to contextual signals that tumour cells receive from their stromal microenvironment. If so, analysis of the gene expression patterns of bulk primary tumour populations may fail to detect the expression of key genes mediating invasiveness and metastasis, if only because they are being transiently expressed in minor subpopulations of cells within such tumours. Additionally, attempts at determining the metastatic propensities of tumours may need to be focused on the genes and proteins that confer responsiveness of primary tumour cells to stromal signals, rather than on the genes and proteins that directly mediate the cellular phenotypes of invasion and metastasis.

METHODS SUMMARY

Cells labelled with GFP or ds-red, or harbouring various overexpression or shRNA constructs, were generated by viral transduction followed by FACS enrichment or antibiotic selection. Xenograft experiments were conducted in nude or NOD/SCID mice and metastasis was estimated using fluorescence microscopy. The levels of cytokines, growth factors and chemokines were assessed by immunoassays. Migration and invasion assays were conducted using transwell chambers. Antibody treatment of tumour-bearing mice was conducted by intraperitoneal injections. See Methods for detailed information regarding cell culture, viral infections, *in vivo* colonization and extravasation assays, RT–PCR, TUNEL and anoikis assays, immunohistochemical and immunofluorescence determinations, western blotting, and antibodies used.

Full Methods and any associated references are available in the online version of the paper at www.nature.com/nature.

Received 13 April; accepted 14 August 2007.

1. Bissell, M. J. & Radisky, D. Putting tumours in context. *Nature Rev. Cancer* **1,** 46–54 (2001).
2. Hall, B., Andreeff, M. & Marini, F. The participation of mesenchymal stem cells in tumor stroma formation and their application as targeted-gene delivery vehicles. *Handb. Exp. Pharmacol.* **180,** 263–283 (2007).
3. Pittenger, M. F. *et al.* Multilineage potential of adult human mesenchymal stem cells. *Science* **284,** 143–147 (1999).
4. Young, H. E. *et al.* Clonogenic analysis reveals reserve stem cells in postnatal mammals: I. Pluripotent mesenchymal stem cells. *Anat. Rec.* **263,** 350–360 (2001).
5. Young, H. E. *et al.* Human reserve pluripotent mesenchymal stem cells are present in the connective tissues of skeletal muscle and dermis derived from fetal, adult, and geriatric donors. *Anat. Rec.* **264,** 51–62 (2001).
6. Fox, J. M., Chamberlain, G., Ashton, B. A. & Middleton, J. Recent advances into the understanding of mesenchymal stem cell trafficking. *Br. J. Haematol.* **137,** 491–502 (2007).
7. Gregory, C. A., Prockop, D. J. & Spees, J. L. Non-hematopoietic bone marrow stem cells: molecular control of expansion and differentiation. *Exp. Cell Res.* **306,** 330–335 (2005).
8. Park, C. C., Bissell, M. J. & Barcellos-Hoff, M. H. The influence of the microenvironment on the malignant phenotype. *Mol. Med. Today* **6,** 324–329 (2000).
9. Nakamura, K. *et al.* Antitumor effect of genetically engineered mesenchymal stem cells in a rat glioma model. *Gene Ther.* **11,** 1155–1164 (2004).
10. Nakamizo, A. *et al.* Human bone marrow-derived mesenchymal stem cells in the treatment of gliomas. *Cancer Res.* **65,** 3307–3318 (2005).
11. Hung, S. C. *et al.* Mesenchymal stem cell targeting of microscopic tumors and tumor stroma development monitored by noninvasive *in vivo* positron emission tomography imaging. *Clin. Cancer Res.* **11,** 7749–7756 (2005).
12. Menon, L. G. *et al.* Differential gene expression associated with migration of mesenchymal stem cells to conditioned medium from tumor cells or bone marrow cells. *Stem Cells* **25,** 520–528 (2007).
13. Komarova, S., Kawakami, Y., Stoff-Khalili, M. A., Curiel, D. T. & Pereboeva, L. Mesenchymal progenitor cells as cellular vehicles for delivery of oncolytic adenoviruses. *Mol. Cancer Ther.* **5,** 755–766 (2006).
14. Khakoo, A. Y. *et al.* Human mesenchymal stem cells exert potent antitumorigenic effects in a model of Kaposi's sarcoma. *J. Exp. Med.* **203,** 1235–1247 (2006).
15. Studeny, M. *et al.* Bone marrow-derived mesenchymal stem cells as vehicles for interferon-β delivery into tumors. *Cancer Res.* **62,** 3603–3608 (2002).
16. Luboshits, G. *et al.* Elevated expression of the CC chemokine regulated on activation, normal T cell expressed and secreted (RANTES) in advanced breast carcinoma. *Cancer Res.* **59,** 4681–4687 (1999).
17. Niwa, Y. *et al.* Correlation of tissue and plasma RANTES levels with disease course in patients with breast or cervical cancer. *Clin. Cancer Res.* **7,** 285–289 (2001).
18. Azenshtein, E. *et al.* The CC chemokine RANTES in breast carcinoma progression: regulation of expression and potential mechanisms of promalignant activity. *Cancer Res.* **62,** 1093–1102 (2002).
19. Robinson, S. C. *et al.* A chemokine receptor antagonist inhibits experimental breast tumor growth. *Cancer Res.* **63,** 8360–8365 (2003).
20. Hillyer, P. & Male, D. Expression of chemokines on the surface of different human endothelia. *Immunol. Cell Biol.* **83,** 375–382 (2005).
21. Thiery, J. P. Epithelial-mesenchymal transitions in tumour progression. *Nature Rev. Cancer* **2,** 442–454 (2002).
22. Toker, A. & Yoeli-Lerner, M. Akt signaling and cancer: surviving but not moving on. *Cancer Res.* **66,** 3963–3966 (2006).
23. Tanaka, T. *et al.* Chemokines in tumor progression and metastasis. *Cancer Sci.* **96,** 317–322 (2005).
24. Mira, E. *et al.* A role for chemokine receptor transactivation in growth factor signaling. *EMBO Rep.* **2,** 151–156 (2001).
25. Qin, X. F., An, D. S., Chen, I. S. & Baltimore, D. Inhibiting HIV-1 infection in human T cells by lentiviral-mediated delivery of small interfering RNA against CCR5. *Proc. Natl Acad. Sci. USA* **100,** 183–188 (2003).
26. West, R. B. *et al.* Determination of stromal signatures in breast carcinoma. *PLoS Biol.* **3,** e187 (2005).
27. Allinen, M. *et al.* Molecular characterization of the tumor microenvironment in breast cancer. *Cancer Cell* **6,** 17–32 (2004).
28. Balkwill, F. Cancer and the chemokine network. *Nature Rev. Cancer* **4,** 540–550 (2004).
29. Karnoub, A. E. & Weinberg, R. A. Chemokine networks and breast cancer metastasis. *Breast Dis.* **26,** 75–85 (2006).
30. Palani, A. & Tagat, J. R. Discovery and development of small-molecule chemokine coreceptor CCR5 antagonists. *J. Med. Chem.* **49,** 2851–2857 (2006).

Supplementary Information is linked to the online version of the paper at www.nature.com/nature.

Acknowledgements We thank F. Reinhardt for assistance in animal studies, A. Lu for technical help, J. Yao for SAGE data analysis and the MIT Comparative Pathology Laboratory for immunohistochemical analyses. We are grateful to A. Bernad, X.-F. Qin, D. Baltimore and W. Hahn for providing constructs. We would also like to thank R. Hynes, T. Jacks and R. Goldsby for discussions. A.E.K. is a fellow of the Susan G. Komen Breast Cancer Foundation. R.A.W. is an American Cancer Society Research Professor and a Daniel K. Ludwig Cancer Research Professor. This research is supported by grants from the Breast Cancer Research Foundation (R.A.W.), the Ludwig Trust (R.A.W.), the Susan G. Komen Breast Cancer Foundation (R.A.W.) and the Dana-Farber/Harvard Cancer Center Specialized Program of Research Excellence (SPORE) in Breast Cancer (A.E.K., R.A.W. and K.P.).

Author Contributions A.E.K. conceived and designed this study, and performed most experiments; R.A.W. supervised research; A.E.K. and R.A.W. wrote the manuscript; A.B.D. and R.T. provided human MSCs; A.B.D. helped in *in vivo* CCL5 neutralization; A.S. helped in the Luminex screens; A.P.V. and M.W.B. provided technical support in tissue culture, ELISA, western blot, RT–PCR and soft-agar analyses; G.W.B. performed CCL5 analysis on soft tumour expression data; A.L.R. obtained and classified the clinical specimens; K.P. fractionated the clinical samples and performed SAGE analyses; and A.L.R. performed the microarray analysis on sorted stroma.

Author Information The clinical microarray data on the sorted stroma is deposited at http://www.ncbi.nlm.nih.gov/geo, GSE8977. Reprints and permissions information is available at www.nature.com/reprints. Correspondence and requests for materials should be addressed to R.A.W. (weinberg@wi.mit.edu).

METHODS

Cell lines. The MCF7/Ras[31] and MDA-MB-231 (ATCC HTB-26) cancer cells were infected with pWZL-blasticidin-GFP-expressing retroviral particles and grown in Dulbecco's modified Eagle medium supplemented with 10% calf serum, 100 units ml^{-1} penicillin, 100 μg ml^{-1} streptomycin and 2 mM L-glutamine (complete medium) at 37 °C in 5% CO_2. The MDA-MB-435 and human mammary epithelial cells HMLER[32] were infected with pRRL3-GFP-expressing lentivirus and grown in complete medium or MEGM media with bovine pituitary extract, respectively. Bone-marrow-derived human MSCs were isolated from hip aspirates of healthy volunteers, propagated as previously described[33], and used between the 4th and 8th passages. Three different batches of MSC cultures derived from three different donors were assayed and exhibited consistent results. MSCs expressing GFP or ds-red were generated by lentiviral (pRRL3-GFP) or retroviral ds-red (Clontech) particles. WI-38 human embryonic lung fibroblasts (ATCC CCL-75) were grown in Dulbecco's modified Eagle medium supplemented with 10% calf serum and were used before the 20th passage. The MDA-MB-231 cells overexpressing human CCL5 (MDA-MB-231/CCL5) were generated by retroviral infection of parental cells with pLZ-CCL5-IRES-gfp[24] viral particles. Control cultures were infected with pLZ-IRES-gfp retrovirus. WI-38 fibroblasts overexpressing CCL5 were generated by retroviral infection of parental cells with pWZL-Blasticidin-CCL5-expressing viral particles. MDA-MB-231 cells lacking CCR5 expression were generated by lentiviral infection of parental cells with FG12-siCCR5(809) or FG12-siCCR5(186) viral particles[25]. MDA-MB-231 cells infected with the control FG12 vector harbouring shRNA against bacterial *lacZ* (FG12-silacZ) were used as a control cell line. All infected cells were enriched for GFP expression using FACS.

Animal studies. All mouse studies were performed under the supervision of MIT's Division of Comparative Medicine and were done in accordance with protocols approved by the Institutional Animal Care and Use Committee. Athymic female nude (NCR nude, nu/nu) mice were purchased from Taconic Laboratories and NOD/SCID mice were bred in-house. Animals were housed under pathogen-free conditions and were given autoclaved food and water *ad libitum*. For xenograft experiments, cancer cells were implanted alone, or were mixed with MSCs or WI-38 fibroblasts and injected subcutaneously into recipient animals as previously described[32]. Nude mice were used at ~10–13 weeks of age and received sub-lethal 400 rad of γ-radiation using a dual ^{137}caesium source 18–24 h before injection. Female NOD/SCID mice were used at 12–14 weeks of age. Tumours were measured twice weekly using precision calipers. Tumour volume was calculated as $4/3\pi r^3$ where r is the estimated radius. Tumours were dissected out at the end of the experiments and weighed.

CFU-F studies. Tumour xenografts were implanted in recipient NOD/SCID females and allowed to grow for 4 weeks. Tumours were then excised, treated with collagenase and the GFP-negative mouse stroma was isolated from the GFP-positive cancer cells using FACS. CFU-F culture assays were performed on the sorted mouse stroma as standard (Stem Cell Technologies). Colonies were stained 14 days later using Giemsa stain and enumerated under light microscopy.

Quantification of lung metastasis. Mice were killed using CO_2 asphyxiation and entire lungs were removed, washed in PBS, and placed in ice-cold Hank's buffer (HBSS, Gibco). Excised lungs were immediately dissected into their various lobes under bright-field microscopy and examined under fluorescence microscopy within 12 h of excision. This circumvents tissue autofluorescence (typically apparent ~24–36 h after necropsy), which greatly masks the GFP signal from the disseminated cancer cells. Lung metastasis burden was estimated as the number of GFP-positive colonies observed under fluorescence microscopy. The lung metastasis index for each mouse was calculated as the ratio of the number of GFP-positive colonies observed in the lungs divided by the mass of the primary tumour (in grams). Indices were pooled within each cohort and were expressed as mean ± s.e.m.

Immunoassays. The levels of cytokines, growth factors and chemokines in the culture media were assessed by xMAP Bio-Plex cytokine array (Bio-Rad Life Sciences) using a Luminex 100 plate reader (Bio-Rad Life Sciences) according to the manufacturer's protocols. The levels of CCL5 in the various culture supernatants were measured using enzyme-linked immunosorbent assay (ELISA; R&D systems).

RT–PCR analysis. GFP-labelled MSCs were admixed to MDA-MB-231 cells and implanted subcutaneously in recipient NOD/SCID mice. Four weeks later, tumours were excised, and GFP-labelled MSCs were purified using FACS and processed for RT–PCR analysis for CCL5 using the following forward and reverse primers: CCL5-left, 5′-TGCAGAGGATCAAGACAGCA-3′, and CCL5-right, 5′-GAGCACTTGCCACTGGTGTA-3′. RT–PCR on cultured cells was performed as standard.

Migration assays. Cancer cells were seeded in the upper well of a 24-well transwell Boyden chamber (8 μm pore size; Costar) and migration was assessed 18 h later. For MSC migration assays, MSCs were layered in the upper well of a 24-well transwell chamber and allowed to migrate towards cell-free media derived from MCF7/Ras or MDA-MB-231 cells placed in the bottom wells. Membranes were processed as standard. Migrating cells were stained with crystal violet and counted using bright-field microscopy.

Extravasation assays. GFP-labelled cancer cells were infused into the circulation of recipient NOD/SCID mice through tail-vein injection. Forty-eight hours later, mice were anaesthetized and their thoracic cage opened. Texas-red lectin (to visualize blood vessels; from *Lycopersicon esculentum*, Vector) was then introduced into the left cardiac ventricle, followed by 4% PFA and then 20 ml of cold PBS. Frozen lung tissue was prepared and sections were processed for fluorescence microscopy as standard.

Anchorage-independent growth assays. We carried out soft agar assays as described previously[34].

Western blot analyses. Western blotting was done using standard protocols. We used primary antibodies against phosphorylated S473-Akt (4051, Cell Signaling), Bcl-XL (2762, Cell Signaling), Bcl-2 (2872, Cell Signaling), β-actin (ab8224, Abcam), CCR5 (ab21653, Abcam), cleaved caspase-3 (9664, Cell Signaling), PARP (9542, Cell Signaling), N-cadherin (205606, Calbiochem) and vimentin (V9, NeoMarkers). We used goat antibodies to mouse (115-035-146) and to rabbit (111-035-144) conjugated with horseradish peroxidase as secondary antibodies (Jackson Immunoresearch), and developed the blots using ECL (Dura, Pierce).

Immunohistochemistry. Immunohistochemical analyses were performed on formalin-fixed, paraffin-embedded tissues. Sections (4-μm thick) were deparaffinized, re-hydrated and subjected to antigen retrieval procedures as described previously[35].

Immunofluorescence. Cells were plated on 0.2% gelatin-coated coverslips in complete medium overnight, washed in PBS, permeabilized in 0.1% Triton-X100, blocked in 1% BSA/10% serum, fixed in 3.6% PBS-buffered paraformaldehyde, and processed for indirect immunofluorescence analyses as standard.

Anti-CCL5 treatment. MDA-MB-231 cancer cells alone or admixed with MSCs were injected subcutaneously into recipient mice. Anti-CCL5 (32 μg per mouse; AF-278-NA, R&D) or control isotype IgG (32 μg per mouse) antibodies were injected into the peritoneum 48 h after tumour implantation and twice weekly for the duration of the experiments (10 weeks).

Anoikis assays. Cancer cells were starved in 1% IFS/DME for 24 h, then trypsinized and suspended in serum-free media. Tubes were continuously rotated at 37 °C for the duration of the experiments. Viable cells were counted using the Trypan blue exclusion assay.

TUNEL assays. Apoptosis quantification analysis was performed using the TUNEL assay as recommended by the manufacturer (Roche), with the exception that the GFP-labelled MDA-MB-231/control and MDA-MB-231/CCL5 cells were fixed for 60 min in ice-cold methanol (instead of 15 min in 3.6% paraformaldehyde) to quench the GFP fluorescence.

Gene expression analysis. Expression ratios (relative to reference mRNA) and classes of soft-tissue tumours were obtained from ref. 26 via NCBI GEO (GSE4305). CCL5 expression was calculated as the mean of probes for IMAGE:1325655 and IMAGE:840753. For Affymetrix gene expression analysis, RNA extraction, cRNA synthesis and hybridization to Human Genome U133 Plus 2.0 Arrays were performed as described previously[36]. Raw expression data obtained using Affymetrix GENECHIP software was normalized and analysed using DNA-Chip Analyser (dChip) custom software (W. H. Wong and C. Li, http://www.dChip.org/). Array probe data were normalized to the mean expression level of each of the three CCL5 probes across stromal samples prepared from a set of 15 normal and 7 IDC (invasive ductal carcinoma) specimens. Leukocyte- and endothelial cell-free stroma was isolated as previously described[27]. Comparisons between 'Normal' and 'Tumour' (IDC breast stroma) were performed using the dChip 'Compare Sample' function. SAGE data were obtained from http://cgap.nci.nih.gov/SAGE/AnatomicViewer and performed as previously described[27]. Data were normalized, log-transformed and clustered using average linkage uncentred analysis. Detailed purification methodologies and sample identification numbers have been previously published[27].

31. Orimo, A. *et al.* Stromal fibroblasts present in invasive human breast carcinomas promote tumor growth and angiogenesis through elevated SDF-1/CXCL12 secretion. *Cell* **121**, 335–348 (2005).
32. Elenbaas, B. *et al.* Human breast cancer cells generated by oncogenic transformation of primary mammary epithelial cells. *Genes Dev.* **15**, 50–65 (2001).
33. Lodie, T. A. *et al.* Systematic analysis of reportedly distinct populations of multipotent bone marrow-derived stem cells reveals a lack of distinction. *Tissue Eng.* **8**, 739–751 (2002).

34. Hahn, W. C. *et al.* Creation of human tumour cells with defined genetic elements. *Nature* **400,** 464–468 (1999).
35. Kuperwasser, C. *et al.* Reconstruction of functionally normal and malignant human breast tissues in mice. *Proc. Natl Acad. Sci. USA* **101,** 4966–4971 (2004).
36. Richardson, A. L. *et al.* X chromosomal abnormalities in basal-like human breast cancer. *Cancer Cell* **9,** 121–132 (2006).